Progress In Electromagnetics Research C, Vol. 76, 99–108, 2017

A Miniaturized Bandpass Frequency Selective Surface with High Selectivity Base on Slot Coupling

Shilin Yang*, Qiang Chen, Jiajun Bai, and Yunqi Fu

Abstract—A Ku-band bandpass frequency selective surface (FSS) with high selectivity and miniaturization is proposed in this paper. We use two metallic strips and one slot to design the frequency selective surface structure which contains both electrical and magnetic couplings. A metallic via is introduced in the FSS element for miniaturization. With the via inserted at the end of the metallic strip, the FSS unit size is reduced to half compared to that without via inserted. To investigate the operating principle of the slot-coupled FSS, an equivalent-circuit model is given and analysed using the odd- and even-mode method. The constructed out-of-phase signal path causes two transmission zeros (TZs) near the skirts of the narrow pass band, thereby enhancing the selectivity. A prototype of the proposed FSS operating at 16 GHz is fabricated and measured. The measured results agree well with the full-wave and circuit simulation results, thus verifying the FSS design.

1. INTRODUCTION

Frequency selective surfaces (FSSs) can be viewed as filters with radiative ports [1], which are generally realized using a planar periodic structure. They can also be used as transmitarrays [2], reflectarrays [3] and substrates of antennas [4]. Recently, FSS with flattop, high selectivity and miniaturization is increasingly becoming a hot research spot. High order frequency response can be realized by using multilayer FSS structure [5], but there are no transmission zeros at finite frequencies. A genetic algorithm has been used to design a FSS structure with transmission zeros [6], while the FSS structure optimized by the genetic algorithm is usually complicated. An alternative method uses three-dimensional (3-D) structures [7]. However, it is hard to achieve low profile and light weight, and it is usually hard to be fabricated. These factors need to be considered in practical applications. In [8], an FSS structure was designed as antenna-filter-antenna modules which focus on making higher order FSS by integrating coplanar-waveguide resonators into coupling slots. It can also make transmission zeros. However, it is of large unit size, which suffers from grating lobes for oblique incidence. In [9], a feasible method is given to realize transmission zeros by combining electrical coupling and magnetic coupling. In fact, the slot coupling method has already been used in [10]. For these reported FSS structures, there is no TZ appearing near the skirts of the passband. The FSS units sometime need to have small size for practical applications. To solve this problem, several methods have been reported such as using spiral shapes [11], adding capacitive or inductive bulk components [12], or fabricating a complex pattern [13]. Although these methods are useful, they may require additional cost for creating new elements or adding bulk components.

In this paper, a slot-coupled Ku-band bandpass FSS structure is proposed. This FSS structure shows advantages of high selectivity and low profile. The FSS structure is constructed by two metallic strips with lengths of quarter-wavelength and one coupling slot. A metallic via is used to connect the

Received 15 May 2017, Accepted 21 July 2017, Scheduled 31 July 2017
* Corresponding author: Shiling Yang (Yang_shilinnudt@163.com).
The authors are with the College of Electronic Science and Engineering, National University of Defense Technology, Changsha 410073, People's Republic of China.

two metallic strips on different layers. This method has miniaturized the dimensions of the unit cell compared with a half-wavelength resonator unit cell. Based on this method, the FSS original resonator operating model is not changed, and no bulk components are required. Detailed analysis about the operating principle of the FSS based on coupled filter theory [14] is also presented. The relationship between the physical dimensions of the FSS structure and the transmission zeros is thoroughly analysed. The FSS structure is fabricated and measured. The measured results agree well with simulated ones.

2. SLOT-COUPLED FSS STRUCTURE

Figure 1 shows the side view and 3D view of the slot-coupled FSS structure. As seen, the slot-coupled FSS is constructed of three metal layers and two dielectric substrates. Rogers RO3035 with relative permittivity of 3.5 and loss tangent of 0.0015 is used to support the three-layered structure. The metallic strips on the top and bottom surfaces have the same physical dimensions and are connected by a metallic via. A rectangular coupling slot is etched in the middle layer.

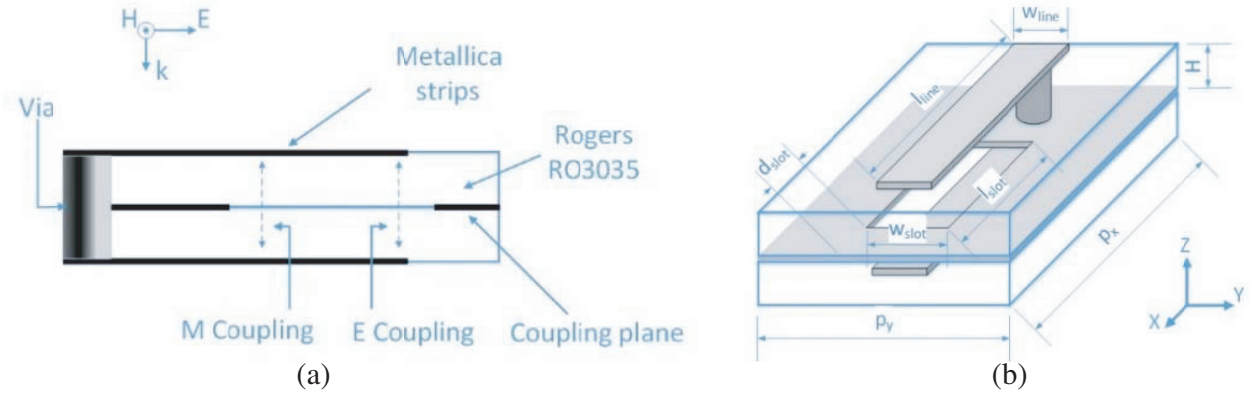

Figure 1. Proposed Ku-band FSS. (a) Side view of the FSS. (b) The 3-D view of the FSS unit cell. (Physical dimension: $p_x = p_y = 4\,\text{mm}$, $h = 0.508\,\text{mm}$, $l_{\text{line}} = 2.8\,\text{mm}$, $w_{\text{line}} = 0.8\,\text{mm}$, $w_{\text{slot}} = 1.2\,\text{mm}$, $l_{\text{slot}} = 1.8\,\text{mm}$, $d_{\text{slot}} = 0.5\,\text{mm}$).

The length of the metal strip resonator can be determined by the microstrip transmission line equation $l = \theta \cdot \lambda_0 / 2\pi\sqrt{\varepsilon_{re}}$ (λ_0 is the free space wavelength at center frequency, and ε_{re} is the effective dielectric constant of the substrate). The electromagnetic coupling is controlled by the dimensions of the coupling slot (w_{slot} l_{slot}) and the position of the coupling slot (d_{slot}). Adjusting these parameters can achieve the desired frequency response.

The slot-coupled FSS structure is simulated under normal incident wave by CST using Floquet boundary. The direction of E-field is parallel with the strip resonator. Inspection of Fig. 1(a) shows that all the electrical E and magnetic M couplings can exist between the top and bottom resonators through the middle coupling slots. Due to the cancelling effect of the constructed paths, multiple transmission zeros can be generated at finite frequencies. Detailed interpretation of the coupling analysis will be given later by an equivalent-circuit model and full-wave electromagnetic simulation.

A traditional half-wavelength metallic strip has a choice to be a resonator in FSS design, but it has large unit size. This paper adopts a method of adding a metallic via at the end of the metallic strips to solve the problem. The E-field and induced current distribution on the half-wavelength element at 16 GHz is shown in Fig. 2(a). It can be seen that the electric field at the middle of the half-wavelength metallic strip is nearly zero, so when inserting a via at the middle of the strip, the operating model does not change. Fig. 2(b) depicts the distribution of a modified quarter-wavelength element. It can be seen that the half-wavelength and quarter-wavelength elements have almost the same E-field and current distribution. This method can reduce unit size to half, thereby realizing miniaturization of the structure. Fig. 3(a) shows that the two elements have similar frequency responses. Strong currents are induced around the metallic via. Magnetic coupling can be generated between the resonators through the coupling slot. The electric field at the end of the metallic strips around the coupling slot is relatively

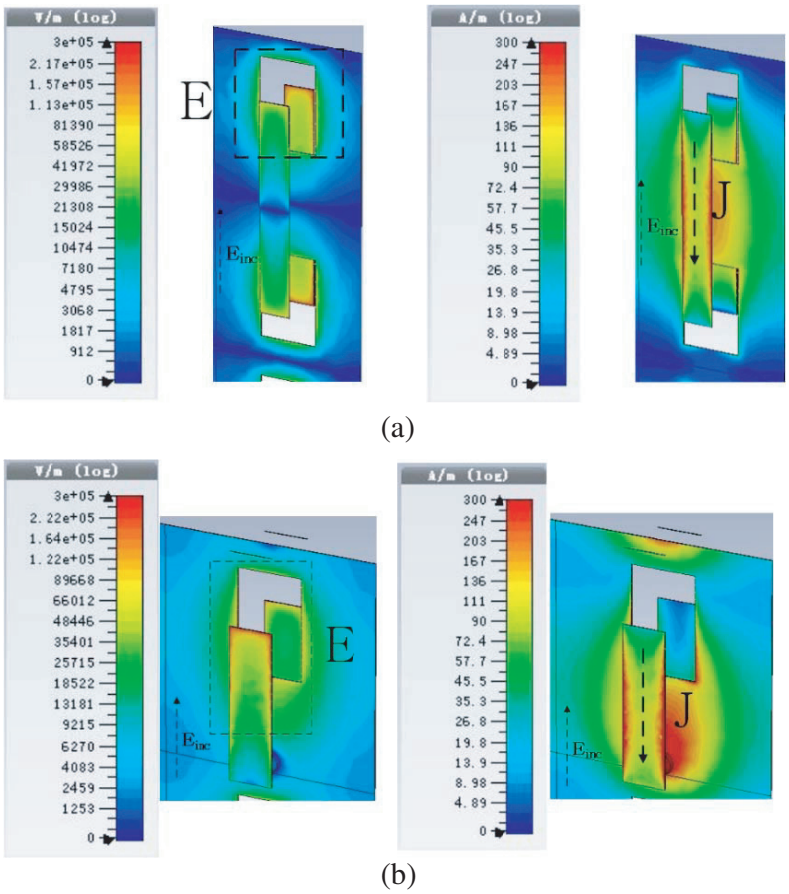

Figure 2. E-field and induced current distribution at 16 GHz. (a) Half-wavelength element. (b) Quarter-wavelength element.

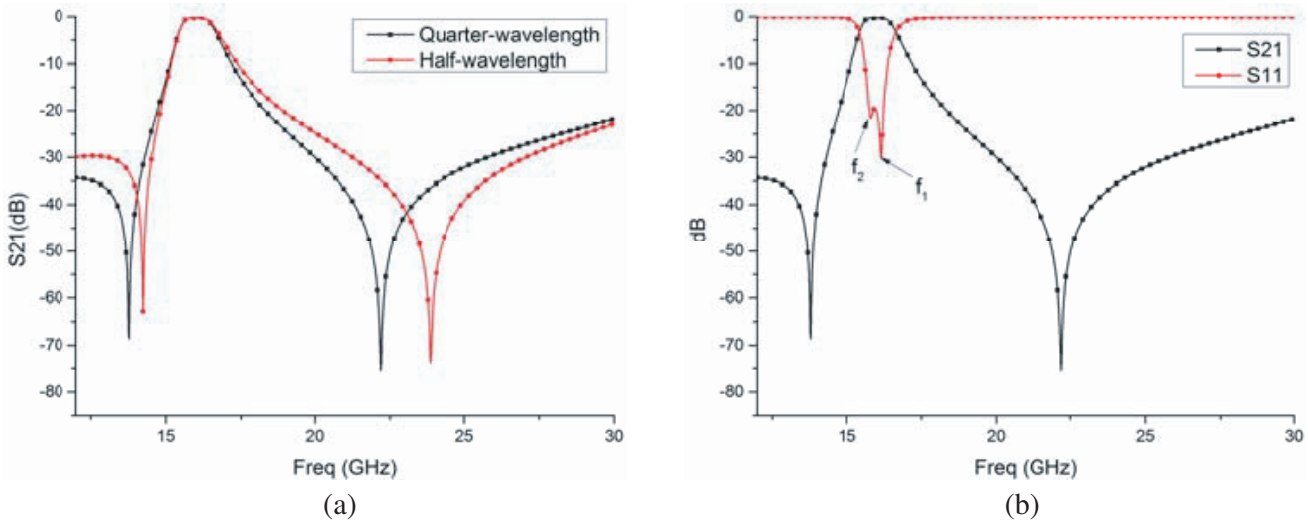

Figure 3. Frequency response (a) two elements compare, (b) quarter-wavelength element frequency response S_{11} and S_{21}.

strong, which enhances the electrical coupling. Because of the electrical coupling and magnetic coupling, two transmission zeros can be generated.

Figure 3(b) gives the frequency response of the FSS. The simulation result shows that the FSS has a flattop at the desired frequency with two transmission poles and a high out-of-band rejection with two transmission zeros. From [15], the closely coupled FSS structure exhibits a narrow bandpass response with two transmission poles in the passband. The first transmission pole f_1 is due to the individual resonator, whereas the other, f_2, appears as a combined effect of the resonators and the coupling slot.

3. FSS STRUCTURE ANALYSIS

3.1. Equivalent-Circuit Model Analysis

In order to explain the operating principle of the slot-coupled FSS, an equivalent-circuit model for the FSS structure is given in Fig. 4(a). For simplicity, all losses are not considered in this circuit model. The two series LC branch circuit represents the metallic strips resonators. The parallel L_{slot} C_{slot} circuit represents the middle coupling slots. Free space on each side of the FSS is modeled with semi-infinite transmission lines with characteristic impedance of $Z0 = 337\,\Omega$. Because the via inserted has no influence on the electric field, the two substrates (Rogers RO3035) are modeled as two short transmission lines with length of $L_s = H$ and characteristic impedance of $Z_s = Z_0/\sqrt{\varepsilon_r}$. The E coupling and M coupling are denoted by the mutual capacitance (C_{m1} C_{m2}) and the mutual inductance (L_{m1} L_{m2}). The physical dimension of the coupling slot influences the values of the parallel L_{slot} C_{slot} circuit, the mutual capacitance and the mutual inductance.

Because of the small values of C_{m2} and L_{m2} (compared with C_{m1} and L_{m1}), they can be ignored in

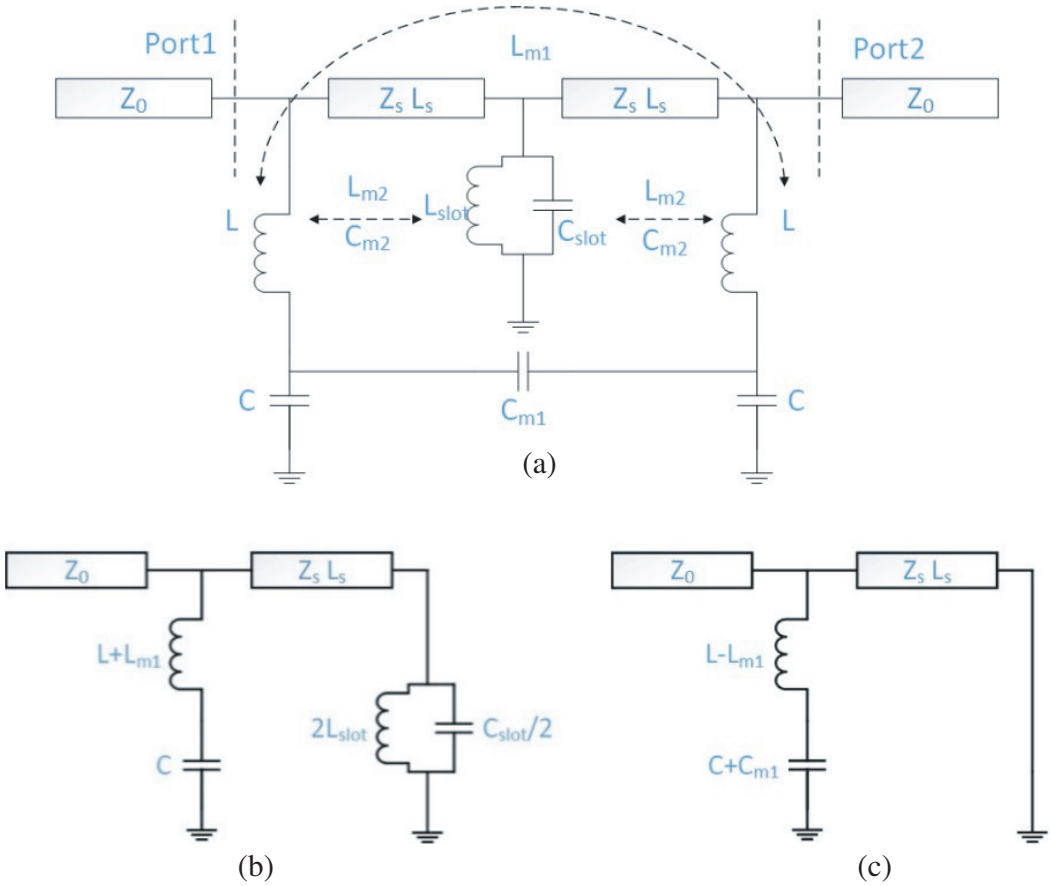

Figure 4. (a) Equivalent-circuit model of the FSS. (b) Even-mode circuit. (c) Odd-mode circuit.

the analysis. As we can see, there are three possible signal paths, including the electrical and magnetic coupling paths (through C_{m1} and L_{m1}) and the signal path directly through the coupling slots (parallel L_{slot} C_{slot} circuit) being constructed. According to the equivalent-circuit in Fig. 4(a), the odd-mode and the even-mode analysis method [16] is used to analyse the circuit. The odd-mode circuit and even-mode circuit can be obtained and are shown in Figs. 4(b) and (c). Then we can get the input admittances Y_{even} and Y_{odd}. They are derived as:

$$Y_{even} = \frac{\sqrt{\varepsilon_r}}{Z_0}\left[\frac{\frac{2jL_{slot}}{1-\omega C_{slot}L_{slot}} + \frac{Z_0}{\sqrt{\varepsilon_r}}\tan(\beta_s l_s)}{\frac{Z_0}{\sqrt{\varepsilon_r}} + j\frac{2jL_{slot}}{1-\omega C_{slot}L_{slot}}\tan(\beta_s l_s)}\right]^{-1} + \left[\frac{1}{j\omega C} + j\omega\left(L + L_{m1}\right)\right]^{-1}. \tag{1a}$$

$$Y_{odd} = \frac{\sqrt{\varepsilon_r}}{jZ_0\tan(\beta_s l_s)} + \left[\frac{1}{j\omega\left(C + C_{m1}\right)} + j\omega\left(L - L_{m1}\right)\right]^{-1} \tag{1b}$$

where $\beta_s = 2\pi/\lambda$ is the wavenumber (λ is the wavelength). The TZs can be realized by forcing $Y_{\text{even}} = Y_{\text{odd}}$ [15]. Then the TZs frequency ω_a can be obtained. So TZs can be controlled by changing the values of L_{m1} and C_{m1}.

According to Y_{even} and Y_{odd}, the even-mode and odd-mode resonant frequencies are given as follows:

$$f_{even} \approx \frac{1}{2\pi\sqrt{\left(L + L_{m1}\right)C}} \tag{2a}$$

$$f_{odd} \approx \frac{1}{2\pi\sqrt{\left(L - L_{m1}\right)\left(C + C_{m1}\right)}} \tag{2b}$$

The overall coupling coefficient k can be calculated using the classical definition as follows:

$$\begin{aligned} k &= \frac{f_{odd}^2 - f_{even}^2}{f_{odd}^2 + f_{even}^2} \\ &= \frac{\left(L - L_{m1}\right)\left(C + C_{m1}\right) - C_{m1}(L + L_{m1})}{\left(L - L_{m1}\right)\left(C + C_{m1}\right) + C_{m1}(L + L_{m1})} \\ &= \frac{\frac{C_{m1}}{C} - 2\frac{L_{m1}}{L} - \frac{L_{m1}}{L}\frac{C_{m1}}{C}}{2 - \frac{C_{m1}}{C} - \frac{L_{m1}}{L}\frac{C_{m1}}{C}} \end{aligned} \tag{3}$$

The absolute values of the inductive magnetic coupling coefficient k_m and the capacitive electrical coupling coupling coefficient k_e are defined as follows:

$$k_m = \frac{L_m}{L} \tag{4a}$$

$$k_e = \frac{C_m}{C} \tag{4b}$$

So the overall coupling coefficient k can be simplified as:

$$k = \frac{k_e - 2k_m - k_m k_e}{2 - k_e - k_m k_e} \tag{5}$$

From the above formulas, the influence of the magnetic and electrical coupling coefficients to the overall coupling coefficient k can be observed.

The equivalent-circuit model for various incident angles is similar. When discussing the oblique incidence, the effective electrical path length of the wave transmitted through the dielectric substrates will change. A slight change in the parameter value in Fig. 4(a) will occur. In addition, the value of the inductor and capacitor can also slightly change in this case.

The initial values of the main electrical parameters of the circuit model are obtained using the given formulas in [5] and [15], and the final parameter values of the equivalent-circuit are obtained by repeated optimization. Based on the equivalent-circuit model, it is easy to find that the LC circuits

determine the operating frequency. The short transmission line also has an effect on it. The effects of the electrical coupling and magnetic coupling coefficients, k_e and k_m, on the frequency response are simulated by ADS, and it is found that when $k < 0$, the bandpass FSS with the transmission zeros located at the lower and upper side of the bands can be realized. Changing the value of C_{m1} and L_{m1} can control the location of the transmission zeros, and adjusting the coupling strength can get the desired bandwidth. The results are given in Fig. 5. It can be seen that the passband with insertion loss less than 1dB is from 15.65 GHz to 16.35 GHz. The minimum insertion loss is 0.25 dB. There are two transmission zeros located at 13.85 GHz and 22.64 GHz, and its performance on out-of-band rejection is excellent.

3.2. Parameters Analysis

According to the equivalent circuit analysis in Section 3.1, it can be seen that the value of the series LC maps to the metal strip resonator physical size (l_{line} and w_{line}). Due to the coupling between the unit and the position of the coupling slot (d_{slot}), the value of C is influenced by several dimensions (l_{line}, w_{line} and d_{slot}). The values of C_{slot} and L_{slot} are determined by l_{slot} and w_{slot}. Furthermore, the

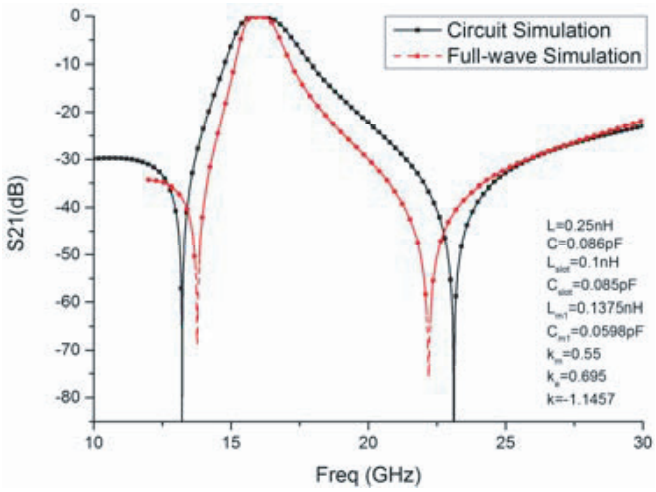

Figure 5. Circuit simulation result and full-wave simulation result.

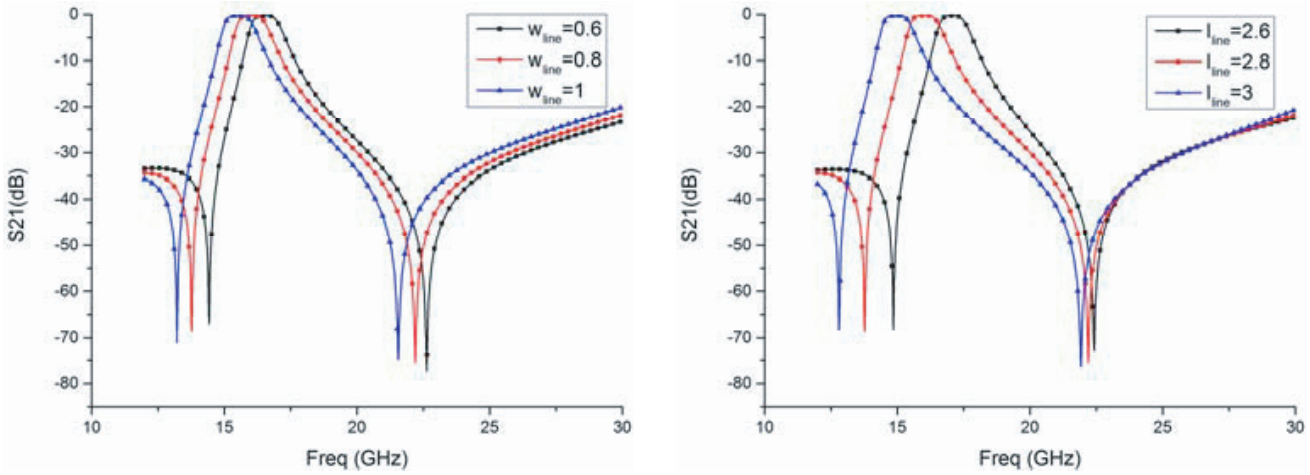

Figure 6. Effects of the metallic strips size on the transmission response. (a) Strips length l_{line}. (b) Strips width w_{line}.

coupling capacitance C_m value is determined by w_{slot}, d_{slot} and w_{line}, and the coupling inductance L_{m} value is determined by w_{slot}, l_{slot}, d_{slot} and l_{line}.

This part mainly focuses on the influence of the physical dimension of the structure on the passband and transmission zeros. Figs. 6(a), (b), Figs. 7(a), (b) and (c) show the effects of the slot and strip size, l_{slot}, w_{slot}, d_{slot}, w_{line} and l_{line}, on the frequency response and location of the transmission zeros.

The physical dimensions of the strips, w_{line} and l_{line}, determine the center frequency of the FSS. At the same time, the fringe capacitor caused by the edge of the strip and the location of the slot also influences the center frequency, and l_{line} also determines the location of the first transmission zero. The result is given in Figs. 6(a) and (b). Based on the results, the desired operating frequency and location of the first transmission zero can be optimized by adjusting w_{line} and l_{line}.

The physical dimension of slot w_{slot} can affect the mutual capacitance and mutual inductance. So when w_{slot} increases, the two transmission zeros get closer to the passband. It has little effect on the width of the passband. The results are given in Fig. 7(a).

The size of slot l_{slot} mainly determines the equivalent inductance and capacitance of the slot and magnetic coupling. When l_{slot} increases, the location of the first transmission zero goes to a higher frequency, and the location of the second transmission zero basically does not change. The results are given in Fig. 7(b).

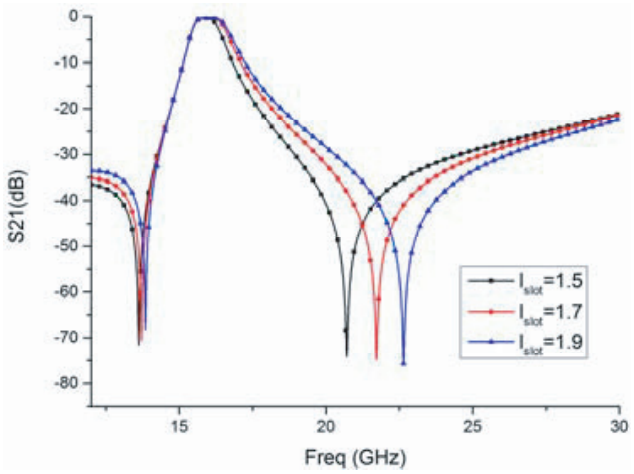

(a)

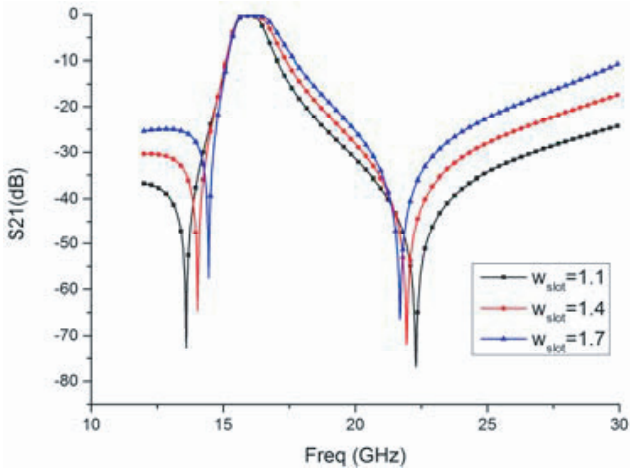

(b)

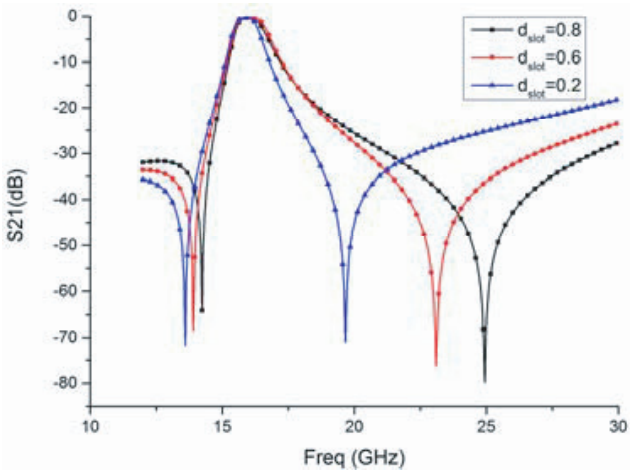

(c)

Figure 7. Effects of (a) coupling slot width w_{slot}, (b) coupling slot length l_{slot}, (c) coupling slot size d_{slot} on the transmission response.

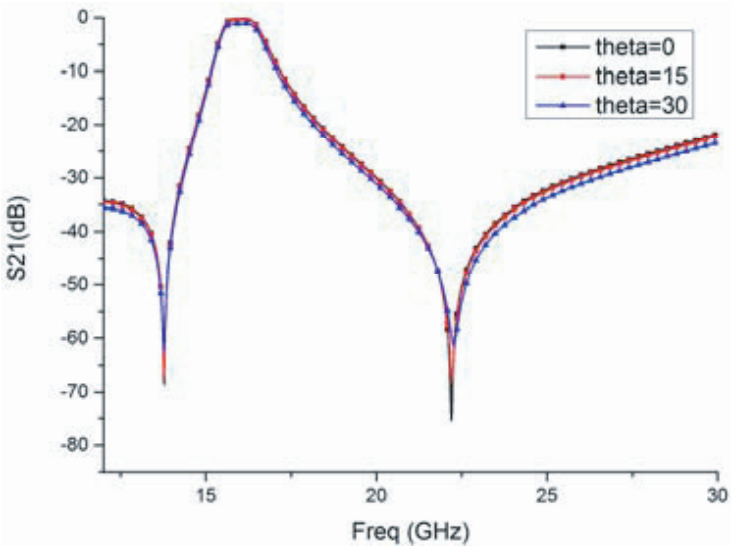

Figure 8. Full-wave simulation result about the angular stability.

The location of the slot, d_{slot}, can change the coupling strength and location of the transmission zeros. When the slot is at the edge of the metallic strips, it mostly produces electrical coupling. When the slot is near the metallic via, it produces magnetic coupling. Covering most part of the metallic strips by slot, both the electrical coupling and magnetic coupling can be obtained. Effects of the coupling slot size d_{slot} is given in Fig. 7(c).

The angular stability is also simulated by the full-wave EM simulation shown in Fig. 8. The simulated frequency responses of the FSS at various incident angles ranging from 0 to 30 degrees are plotted in Fig. 8. It shows that when angle is at 30 degrees, the performance begins to deteriorate with insertion loss 1.13 dB.

4. 16 GHZ SLOT-COUPLED FSS FABRICATION AND MEASUREMENT

Based on the analysis of Section 3, the final design of this type of FSS structure is fabricated (with RO4450 prepreg adding, the thicknesses of the two layers will not be equal. In order to cancel the effect of unequal thicknesses, at the thicker side the length of the metal strip resonator (l_{line}) is reduced by 0.1 mm. The other dimensions are same as shown those in Fig. 1).

A prototype of the FSS structure is fabricated by PCB technology, and its performance is measured. The prototype is composed of two layers of Rogers 3035 substrates and a layer of Rogers 4450F prepreg (0.102 mm). The overall thickness of the whole FSS structure is 1.1 mm (0.06λ, λ is the wavelength in free space). Fig. 9(a) shows the whole structure of the FSS. The whole size of the FSS array is 300 mm $\times$ 300 mm, which contains 75×75 elements. As shown in Fig. 9(b), the FSS sample is measured in an anechoic chamber using two standard antennas and Keysight vector network analyser (VNA) N5244A. Because the measurement should cover a wideband, two types of standard antennas with operating frequencies of 1 GHz–18 GHz and 16 GHz–27 GHz are used. The transmitting antenna and receiving antenna are fixed on a wooden tripod, and the FSS structure is fixed on a rotatable tripod. In order to reduce the multipath effect, the time gate function of the VNA is employed.

The measured frequency responses at normal incidence are given in Fig. 10, together with the full-wave EM simulation and equivalent-circuit simulation results. As observed, the measured results agree well with the full-wave EM simulated ones, which shows that the FSS structure exhibits bandpass characteristics at the desired operating frequency. The two finite transmission zeros appear clearly in the lower and upper frequency regions outside the passband, thus increasing the frequency selectivity.

The measured insertion loss is 0.46 dB (0.26 dB in full-wave EM simulation), and the center frequency is 15.67 GHz (16.01 GHz in full-wave EM simulation). The measured 1-dB bandwidth is 764 MHz from 15.3 GHz to 16.064 GHz (840 MHz from 15.598 GHz to 16.438 GHz). The measured two

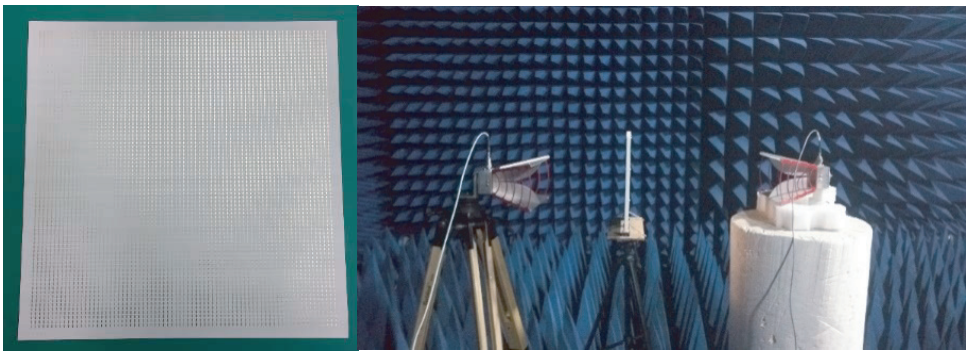

(a) (b)

Figure 9. (a) Fabricated 16 GHz FSS sample. (b) Measurement setup.

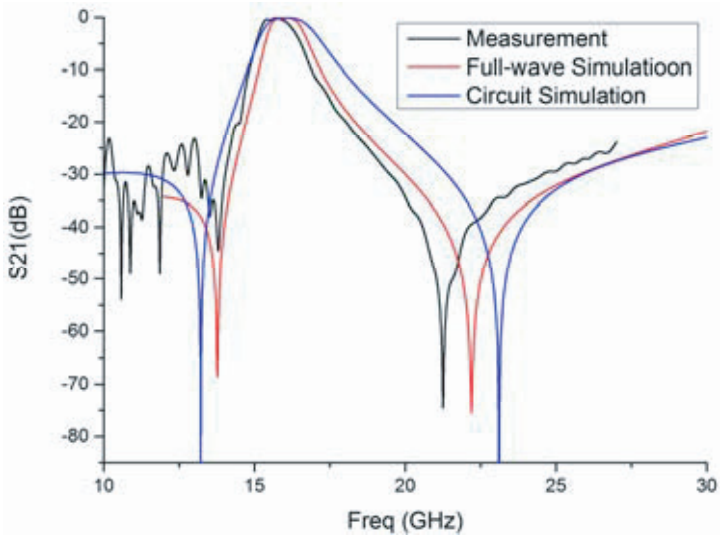

Figure 10. Comparison results.

transmission zeros are located at 13.79 GHz and 21.25 GHz, respectively (13.77 GHz and 22.2 GHz in full-wave EM simulation).

The measured results show that the center frequency is shifted to a lower frequency slightly, and the transmission zero is offset slightly. This may be caused by the fabrication errors related to the center frequency and coupling coefficients [17]. Nevertheless, this discrepancy is within the acceptable level.

5. CONCLUSION

This work has applied slot coupling to realize a Ku-band FSS with high-selectivity. The FSS has an arrow passband with two transmission zeros, which can be controlled separately, in the lower and upper frequencies outside the passband. For the minimization of the structure, a metallic via is used in the structure to construct quarter-wavelength resonators. An equivalent-circuit model is used to analyze the slot-coupled FSS structure, using the odd- and even-mode to analyze the electrical and magnetic couplings and obtain the overall coupling coefficient k. Furthermore, based on the full-wave simulation, the relationship between physical dimensions of the FSS structure and the location of the transmission zeros is given. The relationship can guide the slot-coupled FSS design in the future. The numerical analysis and experimental results indicate that the FSS structure design is a choice for achieving high-selectivity bandpass response with transmission zeros locating either side of the passband.

REFERENCES

1. Behdad, N., "A second-order band-pass frequency selective surface using non-resonant sub-wavelength periodic structures," *Microw. Opt. Technol. Lett.*, Vol. 50, No. 6, 1639–1643, Jun. 2008.
2. Al-Joumayly, M. and N. Behdad, "Wideband planar microwave lenses using sub-wavelength spatial phase shifters," *IEEE Transactions on Antennas and Propagation*, Vol. 59, No. 12, 4542–4552, Dec. 2011.
3. Encinar, J. A., "Design of two-layer printed reflectarrays using patches of variable size," *IEEE Transactions on Antennas and Propagation*, Vol. 49, No. 10, 1403–1410, Oct. 2001.
4. Munk, B. A., *Frequency Selective Surfaces: Theory and Design*, Wiley, New York, 2000
5. Al-Joumayly, M. A. and N. Behdad, "A generalized method for synthesizing low-profile, band-pass frequency selective surfaces with non-resonant constituting elements," *IEEE Transactions on Antennas and Propagation*, Vol. 58, No. 12, 4033-4041, 2010.
6. Ohira, M., H. Deguchi, M. Tsuji, and H. Shigesawa, "Novel waveguide filters with multiple attenuation poles using dual-behavior resonance of frequency-selective surfaces," *IEEE Trans. Microw. Theory Techn.*, Vol. 53, No. 11, 3320–3326, Nov. 2005.
7. Tamijani, A. A., K. Sarabandi, and G. M. Rebeiz, "Antenna-filter-antenna arrays as a class of bandpass frequency-selective surfaces," *IEEE Trans. Microw. Theory Techn.*, Vol. 52, No. 8, 1781–1789, Aug. 2004.
8. Li, B. and Z. Shen, "Three-dimensional bandpass frequency selective structures with multiple transmission zeros," *IEEE Trans. Microw. Theory Techn.*, Vol. 61, No. 10, 3578–3589, Oct. 2013.
9. Tardy, I., C. H. Chan, and J. S. Yee, "Analysis of Yee frequency selective surface," *IEEE Antenna Propag. Soc. Symp. Dig.*, Vol. 1, 196–199, London, ON, Canada, 1991.
10. Chan, C. H., "Novel terahertz dual-polarized frequency selective surface with high frequency selectivity," *IEEE 2014 International Symposium on Antennas and Propagation (ISAP)*, 2014.
11. Yang, G., T. Zhang, W. Li, and Q. Wu, "A novel stable miniaturized frequency selective surface," *IEEE Antennas Wireless Propag. Lett.*, vol. 9, 1018–1021, Nov. 2010.
12. Liu, H. L., K. L. Ford, and R. J. Langley, "Design methodology for a miniaturized frequency selective surface using lumped reactive components," *IEEE Transactions on Antennas and Propagation*, Vol. 57, No. 9, 2732–2738, Sep. 2009.
13. Yu, Y.-M., C.-N. Chiu, Y.-P. Chiou, and T.-L. Wu, "A novel 2.5-dimensional ultraminiaturized-element frequency selective surface," *IEEE Transactions on Antennas and Propagation*, Vol. 62, No. 7, 3657–3663, Jul. 2014.
14. Hong, J. S. and M. J. Lancaster, *Microstrip Filters for RF/Microwave Applications*, Wiley, New York, NY, USA, 2001.
15. Lee, C. K. and R. J. Langley, "Equivalent-circuit models for frequency-selective surfaces at oblique angles of incidence," *Proc. Inst. Elect. Eng. — Microw. Antennas Propag. H*, Vol. 132, Part 6, 395–399, Oct. 1985.
16. Ma, K. X., J. G. Ma, K. S. Yeo, and M. A. Do, "A compact coupling controllable filter with separate electric and magnetic coupling paths," *IEEE Trans. Microw. Theory Techn.*, Vol. 54, No. 3, 1113–1119, Mar. 2006.
17. Tyurnev, V. V., "Coupling coefficients of resonators in microwave filter theory," *Progress In Electromagnetics Research B*, Vol. 21, 47–67, 2010.